Article

Compact Multi Bit Slotted C-Scatterer for Threshold Sensitive Chipless Wireless Temperature Sensor

Hatem El Matbouly [1],[*] [ID], Smail Tedjini [1], Konstantinos Zannas [1] and Yvan Duroc [2]

[1] Laboratoire de Conception et d'Intégration des Systèmes (LCIS), Grenoble-INP, Université Grenoble-Alpes, Valence F-26902, France; Smail.Tedjini@grenoble-inp.fr (S.T.); konstantinos.zannas@lcis.grenoble-inp.fr (K.Z.)

[2] Ampère, University Claude Bernard Lyon 1 (UCBL), University of Lyon, Villeurbanne F-69622, France; yvan.duroc@univ-lyon1.fr

[*] Correspondence: hatem.el-matbouly@lcis.grenoble-inp.fr; Tel.: +33-0681-888-695

check for updates

Abstract: This paper presents a novel compact scatterer structure for a passive chipless wireless temperature threshold sensor. The structure is based on a single C-scatterer with multiple embedded slots; each slot forms a sub-scatterer dedicated to resonating in one regulated band. This structure has the advantage of increasing the data capacity without increasing the number of scatterers, which results in a more compact sensor size. The sensing principle is based on the detuning of the resonance frequency peaks of the backscattered signal from the slotted scatterer due to temperature variations. For the first time, this work demonstrates the design of a passive chipless sensor while at the same time respecting the conventional radio frequency (RF) emission regulations. The sensor only exploits the allowed bands: European Telecommunications Standards Institute (ETSI) and Industrial, Scientific and Medical (ISM). Sensitivity measurement results show sensitive characteristics in the order of 10^{-4} GHz/°C in accordance with the theoretical predictions.

Keywords: threshold temperature sensing; chipless technology; electromagnetic scattering

1. Introduction

Many research efforts have been focused on developing chipless RFID (Radio Frequency Identification) tags for sensing and identifying [1,2]. The chipless RFID technology, in which the tags are made only of an antenna (or equivalently so-called in this case, scatterer), offers the advantage of being realizable in a single fabrication process on different types of substrates. For identification applications, different chipless RFID tag structures have been reported with different methods of data encoding such as time, frequency and phase techniques [3–5]. Moreover, chipless RFID tag structures have been demonstrated in sensing applications [6]. The sensing capabilities can be detected in the reader as backscattered signal alterations, power variations, shifts of frequency or phase variations. The chipless approaches are fully passive and enable accurate and low-cost sensors. In addition, they are good candidates for sensing in harsh environments since they do not have integrated electronics. Different demonstrations have been reported for using chipless RFID tag structures as temperature sensors. For instance, temperature sensors based on detuning resonance frequencies of a resonator has been proposed [7,8]. A chipless RFID-based temperature threshold had been reported in 2017 at the IEEE International Conference on RFIDs [9], where NaCl-water solutions were used as the temperature sensitive material. Passive Ultra High Frequency (UHF) RFID systems for temperature sensors have been developed [10] for high temperature sensing. The main drawback of all these chipless sensor approaches is the use of ultra-wideband (UWB) signals. This not only complicates the chipless reader architecture [11], but also requires specific protocols and associated bandwidths that are nonstandard in the RFID field, strongly limit their commercial implementations.

This work introduces a compact C-scatterer as a threshold temperature sensor with sufficient data capacity in Industrial, Scientific and Medical (ISM) frequency bands that is compliant with RF regulation. The sensor structure does not use a sensitive material, but temperature transduction is achieved through the dielectric properties of commercially available substrates. The proposed solution favors the implementation of a RFID chipless sensor in the real world since it increases its compatibility with the commercially available conventional RFID readers. In addition, this solution facilitates the sensor's design and fabrication process due to the lack of additional extra sensitive materials which would require integration development. Such a topic has not yet been proposed and keeps an open door for research and development of a novel compact chipless structure while meeting standards and RF regulations.

The sensor structure is based on a single C-scatterer which is integrated in different resonant slots. The slots are chosen to form sub-scatterers in the original C-scatterer structure. This topology allows multi-bit encoding capabilities without increasing the original size. This structure can be transformed into a sensor if the used substrate is sensitive to an external parameter such as temperature or moisture. The challenge in the studied sensor operating principle is to encode temperature thresholds in multi-bit information while at the same time respecting the RFID and ISM regulations. The sensor structure is designed on a temperature sensitive dielectric substrate which is used as a transducer. Temperature variation introduces a shift in the value of the resonance frequency of the backscattered signal. Depending on the value of the resonance frequency inside or outside a specific frequency band, the power level of the scattered signal shifts from maximum which corresponds to "logic 1" to minimum which corresponds to "logic 0". The choice of the material is based on a sensitivity analysis of temperature for different substrates in the three frequency bands (ETSI, ISM 2.4 GHz and ISM 5.8 GHz). The sensitivity analysis is confirmed by measurement showing sensitive characteristics of the order of 10^{-4} GHz/°C for the designed and realized sensor structure.

2. Materials and Methods

The C-scatterer has been used in recent chipless RFID demonstrations [12]. A single C-scatterer is considered as a quarter-wavelength ($\lambda/4$) resonator with resonance and anti-resonance frequencies. The choice of $\lambda/4$ scatterer has the advantage of having a smaller and more compact sized sensor structure. The basic idea of the proposed chipless temperature threshold sensor is to take advantage of the substrate properties under the influence of temperature in order to detune the resonance frequency of C-scatterers in the selected frequency bands. This exploited property for implementing the sensing functionality can be explained using a generic relationship between a physical length *L* of a quarter-wavelength ($\lambda/4$) C-scatterer and its resonant frequency:

$$f = \frac{c}{4L\sqrt{\varepsilon_r}} \tag{1}$$

where *c* is the speed of light and ε_r is the effective permittivity of the structure.

Although a single C-scatterer can encode information in different forms such as in resonance (or anti-resonance) or in phase, the C-scatterer presented in this work can represent only one bit of information since only resonance or anti-resonance is considered. For multiple resonance frequency scatterers, the main C-structure is repeated with different lengths *L* that correspond to the expected resonance frequency. This results in a less compact structure which has a dimension that is directly proportional to the number of added C-scatterers [13]. For more compact multi bits scatterers, a slotted C-scatterer structure is introduced in this work as described in Figure 1. It consists of one main $\lambda/4$ C-scatterer that resonates in ETSI RFID band. This main C-scatterer is slotted with $\lambda/2$ C1-scatterer which is designed to resonate in the 2.4 GHz ISM frequency band. Furthermore, two slots C2 and C3 are added for achieving a resonance frequency in the 5.8 GHz ISM frequency band. For this frequency, two identical $\lambda/2$ slots (C2 and C3) are introduced for increasing the amplitude of the backscatter signal

and their relative position is chosen in order to maximize the backscattered signal level. The scatterers are designed for a temperature-sensitive dielectric substrate.
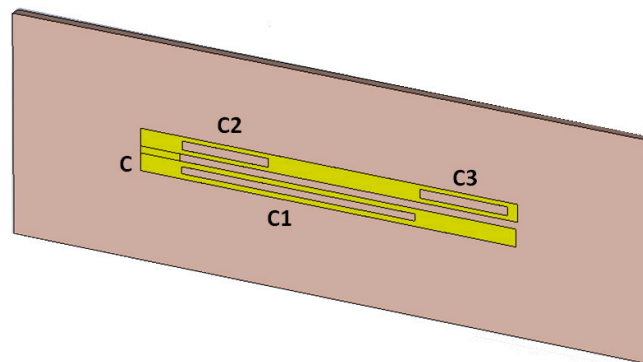

Figure 1. Temperature sensor based on a compact slotted C-scatterer structure exploiting the temperature sensitivity of the dielectric substrate.

As presented through Equation (1), the length of the resonator L and the permittivity ε_r of the substrate strongly determine the resonant frequency. Besides, these two parameters are sensitive to the temperature and play a fundamental role in the sensing operation of the C-scatterer structure. With the objective of achieving a maximum resonant frequencies variation with the temperature, a parametric study is conducted for three separate dielectric substrate cases (RT/duroid 6010.2LM, AD1000, RO3010). The influence of temperature variations on the resonance frequency can be evaluated by applying a variation analysis as follows:

$$\delta f = \left(\frac{\partial f}{\partial L}\right)\delta L + \left(\frac{\partial f}{\partial \varepsilon_r}\right)\delta \varepsilon_r \tag{2}$$

where $\partial f/\partial L$ and $\partial f/\partial \varepsilon_r$ are the partial derivatives of the resonance frequency evaluated at the nominal values of L_0 and ε_r which correspond to the resonance frequency under investigation. δL and $\delta \varepsilon_\gamma$ are the minimum variation of length and permittivity per degree Celsius which are extrapolated from the datasheet information of each substrate under investigation [14]. Even though the contribution of the elongation is of 0.01 order of magnitude in comparison to the contribution the permittivity to the frequency shift, it has been included in this analysis because the elongation has a competing effect on the frequency variation with the permittivity as the temperature increases. Table 1 shows a comparison of the frequency variation δf for the three selected bands resulted from the parametric study in Equation (2).

Table 1. The variation of the resonance frequency per degree Celsius.

Substrate	δf in ETSI 866 MHz Band (GHz/°C)	δf in ISM 2.4 GHz Band (GHz/°C)	δf in ISM 5.8 GHz Band (GHz/°C)
RT/duroid 6010.2LM	1.632×10^{-4}	3.8×10^{-4}	0.0023
AD1000	1.62×10^{-4}	3.4×10^{-4}	0.00218
RO3010	1.572×10^{-4}	3.5×10^{-4}	0.00219

Since a commercial substrate with dielectric temperature dependency is used for this work, the sensitivity is dependent on the dielectric properties of the manufacturer resulting in fixed temperature sensitivity. The substrate chosen for this work is RT/duroid 6010.0LM which has a high dielectric constant ε_r = 10.2, this reduces the resonator size, in addition it has a high coefficient of dielectric constant -425 ppm/°C for significant frequency shift under temperature variation.

3. Results

This section presents the simulation and measurement results for the proposed sensor structure as well as a description of the measurement setup.

3.1. Simulation and Fabrication

The proposed slotted C-scatterer had been simulated for RT/duroid 6010.0LM substrate with the following parameters (ε_r = 10.2, *h* = 1.27 mm, tan δ = 0.0027) and the geometric parameters shown in Figure 2. The simulation was performed using a time domain method by illuminating the structure with a linearly polarized plane wave in y direction (*x-y* plane). The backscatter signal is collected by probes placed 10 cm away from the structure.
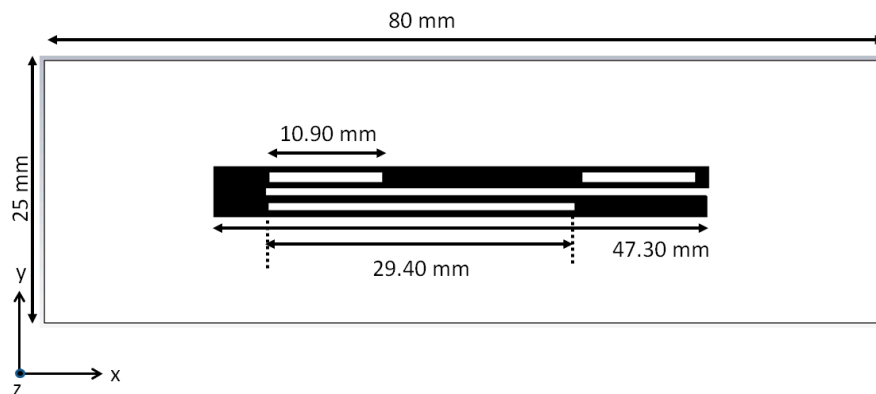
Figure 2. The design parameters for proposed the compact chipless threshold temperature sensor.

Since the reflected power from the structures is of interest, the simulation parameter used to characterize the structures is the monostatic Radar Cross Section (RCS), which is a measure of the structure ability to reflect the incident signal for a given distance. Figure 3 shows the simulation results of the RCS of the proposed sensor structure.
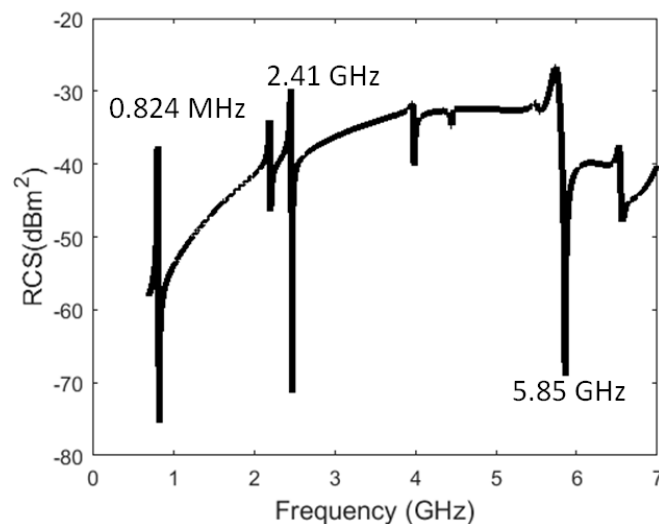

Figure 3. Simulation results of the proposed temperature sensor structure based on the compact C-scatterer. The RCS is measured at 10 cm distance from the structure with plane wave excitation.

Slotted C-scatterers exhibits resonance frequencies corresponding to the three structures C1, C2 and C3 in the bands ETSI, ISM 2.4 GHz and ISM 5.8 GHz respectively. One notices that, other

harmonics are also exhibited, but they are outside bands of interest and therefore are considered as spurious responses.

　　In order to experimentally study the impact of the temperature variation on the resonance frequencies of the sensor as well as deduce the experimental temperature sensitivity of the sensor, the proposed sensor structure has been realized using printed circuit board (PCB) mechanical milling; the fabricated sensor structure is presented in Figure 4.
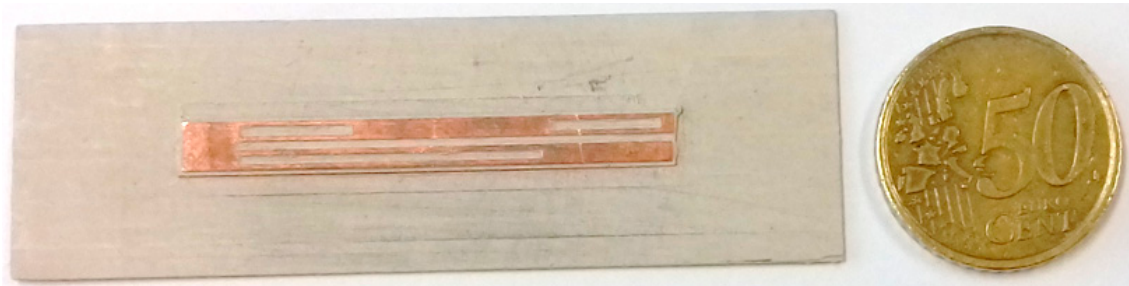

Figure 4. Realized temperature sensor structure based on the compact C-scatterer on a temperature-sensitive dielectric substrate.

3.2. Measurement Setup and Results

　　The experimental setup is shown in Figure 5. The purpose of this measurement is to experimentally evaluate the effect of temperature variations on the resonance frequency in the ETSI and the two ISM bands 2.4 and 5.8 GHz, as well as deducing the sensitivity of the structure.
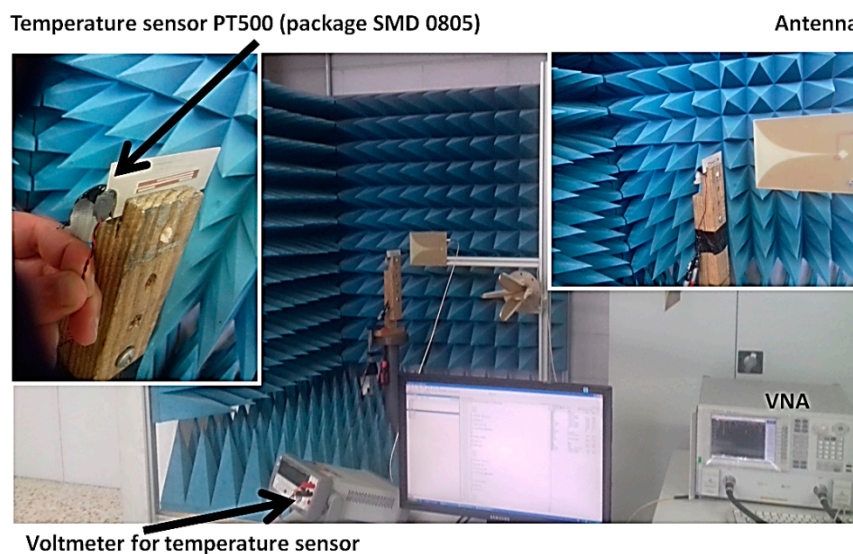

Figure 5. Measurement setup for characterizing the chipless temperature threshold sensor structure.

　　The measurement platform is monostatic, which consists of a linearly polarized Vivaldi antenna (used as the transmitting and receiving antenna) connected to a port of the Agilent E8364C vector network analyzer (VNA). The frequency range of the network analyzer has been chosen to span the ETSI and ISM bands. A power budget has been estimated using $P_r = \frac{P_t G_t}{(4\pi r^2)^2} RCS\, A_{eff}$. for the 10 cm distance where the transmitted power is $P_t = 0$ dBm. The received power is $P_r = -75.2$ dBm for 3 dB antenna gain and RCS of -40 dBm^2, A_{eff} is the effective area of the structure. Given that the dynamic range of the VNA is 120 dB then the ratio $|P_r/P_t|$ lies within the dynamic range. Due to technical issues with the automatized measurement setup, we used 0 dBm as a transmitted power. It is

worth noting that RFID and RF regulations authorize a larger power level (up to 33 dBm). Therefore, the distance can be increased. A commercial temperature sensor PT500 is used to measure the temperature values which is connected to Keysight 34410A digital multi-meter. The measurement system is automated using MATLAB version R2015a interface for synchronizing the reading of the VNA and the temperature sensor. This interface allows measuring the temperature and the corresponding resonance frequency instantaneously.

Since the transmission coefficient is of interest, the measurement procedure starts by measuring the S_{11} parameter of background without the presence of the sensor structure. Then, the sensor structure is placed in front of the antenna and heated using a heat gun to a maximum temperature of around 75 °C. It is allowed to cool down while data acquisition occurs using the computer interface. The effect of the background is removed by subtracting the S_{11} of the background from the S_{11} of the measured sensor. Figure 6 shows the measurement results of the resonance frequency as a function of temperature for the three bands.
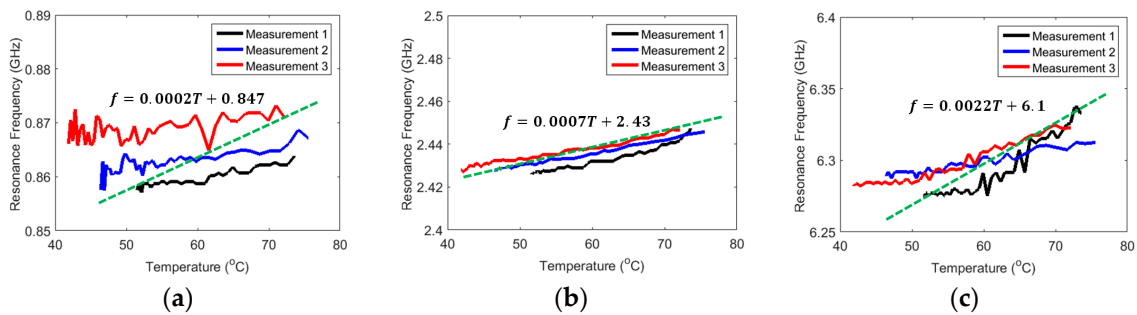

Figure 6. Measurement results of the resonance frequency as a function of temperature for: (**a**) ESTI band; (**b**) ISM 2.4 GHz band; (**c**) ISM 5.9 GHz band.

The measurement is repeated three times; the frequency shift is measured in each band simultaneously during each repetition. The measured frequency shift curves as a function of temperature has been fitted to a linear curve to extract the sensitivity as well as to find the measured nominal value of the resonance frequency of the fabricated sensor structure for comparison with simulation. The linearity has been assumed as an approximation for estimating the sensitivity. Therefore, the relationship between temperature (T) and frequency (f) is written as

$$f = ST + f_0 \tag{3}$$

where f_0 is the nominal resonance frequency and the measured sensitivity S of a resonator is given by [15]

$$S = \left| \frac{\delta f}{\delta T} \right| \tag{4}$$

where δf is the change in the resonance frequency and δT the corresponding variation of the temperature. The sensitivity can be deduced experimentally from the curves shown in Figure 6 since the slope represents sensitivity S.

4. Discussion

A comparison between the simulated and measured resonance frequencies is presented in Table 2. The experimental results at room temperature of the proposed threshold temperature sensor show a resonance frequency error compared to the simulated values.

Table 2. Comparison between the measured and simulated resonance frequencies for the slotted C-scatterer on Duroid6010.2LM substrate.

Frequency Band	Simulation (GHz)	Measured (GHz)	Deviation (GHz)	Deviation (%)
ETSI 866 MHz band	0.824	0.847	0.023	2.7%
ISM 2.4 GHz band	2.41	2.43	0.02	0.8
ISM 5.8 GHz band	5.85	6.1	0.25	4.16

As Table 2 points out, the deviation between the simulated and measured resonance frequencies for ETSI and ISM 2.4 GHz is in the order of 2.7% and 0.8% respectively. However, for ISM 5.8 GHz the error is in the order of 4%. Given that the tolerance of the material has been taken into account in the design of the structure, the reason for this higher percentage of deviation is due to the mechanical fabrication of the structure which altered the thickness of the substrate around the metallic trace of the slotted C2 and C3 scatterers. This affects the thickness of the substrate, resulting in higher deviation especially at high frequency. This can be explained through tolerance analysis of the resonance frequency in ISM 5.8 GHz, taking into account the effect of substrate thickness variation on the effective permittivity. Using the coplanar strip line (CPS) model [16,17], the percentage of deviation in the resonance frequency can be evaluated by applying the analysis as follows:

$$\left| \frac{\delta f}{f_0} \right| = \left| \frac{1}{f_0} \left(\frac{\partial f}{\partial \varepsilon} \right) \delta \varepsilon \right| \tag{5}$$

where f_0 is the nominal value of resonance frequency which in this case is 5.8 GHz. $\delta \varepsilon$ is the tolerance of the effective permittivity due to fabrication which is composed of $\delta \varepsilon_{tolerance}$, given in the datasheet of Duroid6010.2LM substrate ($\delta \varepsilon_{tolerance} = \pm 0.25$). $\delta \varepsilon_h$ is the uncertainty in the permittivity due to the variation of the substrate height, given by [17]

$$\delta \varepsilon_r = \left| \left(\frac{\partial \varepsilon}{\partial h} \right) \delta h \right| \tag{6}$$

where δh is the uncertainty in substrate height due to fabrication tolerance of the Printed Circuit Board (PCB) milling machine and $\partial \varepsilon / \partial h$ is the variation of the permittivity due to the variation of substrate height, which is calculated at the nominal value of substrate height of 1.27 mm. The surface imperfection is due to over etching of the surface around the slots and it is estimated from the fabricated structure to be $\delta h = 0.15$ mm. Using Equations (4) and (5), the estimated deviation of the resonance frequency at 5.8 GHz is

$$\left| \frac{\delta f}{f_0} \right| \times 100 = 4.12\% \tag{7}$$

The sensitivity of the proposed sensor is measured from the slope of the resonance frequency as a function of temperature shown in Figure 6. A comparison between the theoretical and experimental values of sensitivity in each band is presented in Table 3.

Table 3. Comparison between the experimental and theoretical sensitivity for slotted C-scatterer on Duroid6010.2LM substrate.

Frequency Band	Theoretical (GHz/°C)	Experimental (GHz/°C)	Deviation (GHz/°C)
ETSI 866 MHz band	1.632×10^{-4}	2×10^{-4}	0.368×10^{-4}
IMS 2.4 GHz band	3.8×10^{-4}	7×10^{-4}	3.2×10^{-4}
IMS 5.8 GHz band	0.0023	0.0022	1×10^{-4}

Based on the three resonance frequencies, the proposed compact C-scatterer acts as a three bits encoder for temperature ranges. Logic '1' is represented by a resonance within the band, while logic '0'

is represented by a resonance outside the band. The temperature is transduced through the substrate properties into a resonant frequency shift spanning the ETSI and ISM bands. Since these bands do not have the same bandwidth, one expects that the resonance shift will not be the same and hence allow different bit combinations to be assigned to ranges of temperatures. Figure 7 illustrates the principle of temperature threshold encoding.
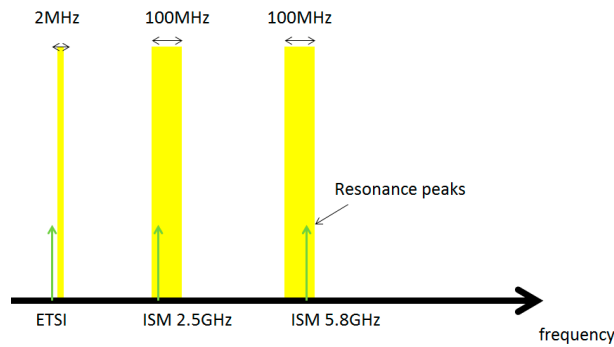

Figure 7. The spectrum of the frequency bands illustrating the principle of temperature threshold coding.

From Figure 6, different temperature thresholds that could be encoded using the proposed slotted C-scatter using a three bits combination. The three-bit binary numbers associated with the temperature range are listed in Table 4.

Table 4. The different bit combination representing the temperature range of the proposed chipless sensor.

Temperature Range	ETSI 866 MHz Band	IMS 2.4 GHz Band	IMS 5.8 GHz Band
$T < 30\,°C$	0	1	1
$45 < T < 60\,°C$	0	1	0
$60 < T < 75\,°C$	1	1	0
$T < 75\,°C$	0	0	0

Having low sensitivity, as in the case of the proposed sensor, is important in threshold sensing since it increases the temperature ranges detected by the sensor and the binary codes associated with it. Having high sensitivity can limit the number of threshold ranges because any small temperature variation will quickly shift the resonance frequency out of the band of interest, especially for ETSI band, hence, limiting the threshold binary code. It is worth noting that for this study four threshold values are encoded in binary format depending on the resonance peak position in the band. However, different bit combinations could be obtained either by engineering the position of the resonance peak in or outside the frequency bands or by extending temperature range to incorporate negative temperatures.

5. Conclusions

In this paper the design of a compact threshold temperature sensor based on a slotted C-scatterer is presented. The proposed concept is based on the integration of several slot resonators in the same C-scatterer for a multi-bit chipless sensor. In order to be compliant with the RF regulation standards, the sensor is designed to operate in the ETSI RFID, ISM 2.5 GHz and ISM 5.8 GHz bands. The operation principle relies on temperature transducing as a frequency, detuning in three radio frequency bands. The sensitivity analysis is confirmed by measurement, showing sensitive characteristics of the order of 10^{-4} GHz/°C for the designed and realized sensor structure. The compact chipless sensor structure has the effect of pushing the trend to implement the chipless RFID sensing solutions in real world applications.

References

1. Tedjini, S.; Karmakar, N.; Perret, E.; Vena, A.; Koswatta, R.; E-Azim, R. Hold the Chips: Chipless Technology, an Alternative Technique for RFID. *IEEE Microw. Mag.* **2013**, *14*, 56–65. [CrossRef]

2. Girbau, D.; Ramos, Á.; Lazaro, A.; Rima, S.; Villarino, R. Passive wireless temperature sensor based on time-coded UWB chipless RFID tags. *IEEE Trans. Microw. Theory Tech.* **2012**, *60*, 3623–3632. [CrossRef]

3. Genovesi, S.; Costa, F.; Monorchio, A.; Manara, G. Phase-only encoding for novel chipless RFID tag. In Proceedings of the 2014 IEEE RFID Technology and Applications Conference (RFID-TA), Tampere, Finland, 8–9 September 2014; pp. 68–71.

4. Ramos, A.; Perret, E.; Rance, O.; Tedjini, S.; Lázaro, A.; Girbau, D. Temporal separation detection for chipless depolarizing frequency coded RFID. *IEEE Trans. Microw. Theory Tech.* **2016**, *64*, 2326–2337. [CrossRef]

5. Herrojo, C.; Moras, M.; Paredes, F.; Núñez, A.; Ramon, E.; Mata-Contreras, J.; Martín, F. Very Low-Cost 80-Bit Chipless-RFID Tags Inkjet Printed on Ordinary Paper. *Technologies* **2018**, *6*, 52. [CrossRef]

6. Vena, A.; Perret, E.; Tedjini, S.; Kaddour, D.; Potie, A.; Barron, T. A compact chipless RFID tag with environment sensing capability. In Proceedings of the 2012 IEEE/MTT-S International Microwave Symposium Digest, Montreal, QC, Canada, 17–22 June 2012; pp. 1–3.

7. Mandel, C.; Jiménez-Sáez, A.; Polat, E.; Schüßler, M.; Kubina, B.; Scherer, T.; Lautenschläger, N.; Jakoby, R. Dielectric ring resonators as chipless temperature sensors for wireless machine tool monitoring. In Proceedings of the 2017 11th European Conference on Antennas and Propagation (EUCAP), Paris, France, 19–24 March 2017; pp. 3912–3916.

8. Noor, T.; Habib, A.; Amin, Y.; Loo, J.; Tenhunen, H. High-density chipless RFID tag for temperature sensing. *Electron. Lett.* **2016**, *52*, 620–622. [CrossRef]

9. Martinez, M.; van der Weide, D. Chipless RFID temperature threshold sensor and detection method. In Proceedings of the 2017 IEEE International Conference on RFID (RFID), Phoenix, AZ, USA, 9–11 May 2017; pp. 61–66.

10. Kamil, J.; Małgorzata, J.; Grażyna, K.; Piotr, J.-M. Passive UHF RFID-Enabled Sensor System for Detection of Product'S Exposure to Elevated Temperature PDF Download. Available online: http://lib-dl.com/ (accessed on 11 June 2018).

11. Jankowski-Mihułowicz, P.; Węglarski, M.; Pitera, G.; Kawalec, D.; Lichoń, W. Development board of the autonomous semi-passive RFID transponder. *Bull. Pol. Acad. Sci. Tech. Sci.* **2016**, *64*, 647–654. [CrossRef]

12. El Matbouly, H.; Zannas, K.; Duroc, Y.; Tedjini, S. Chipless wireless temperature sensor based on C-like scatterer for standard RFID reader. In Proceedings of the 2017 XXXIInd General Assembly and Scientific Symposium of the International Union of Radio Science (URSI GASS), Montreal, QC, Canada, 19–26 August 2017; pp. 1–3.

13. Polivka, M.; Machac, J. Improvement of backscatter properties of C-shaped dipole scatterer for chipless RFID. In Proceedings of the 2014 Asia-Pacific Microwave Conference, Sendai, Japan, 4–7 November 2014; pp. 962–964.

14. RT/Duroid® 6006 & 6010 Laminates. Available online: https://www.rogerscorp.com/acs/products/36/RT-duroid-6006-6010-Laminates.aspx (accessed on 3 May 2018).

15. Fraden, J. *Handbook of Modern Sensors: Physics, Designs, and Applications*, 4th ed.; Springer: New York, NY, USA, 2010; ISBN 978-1-4939-0040-4.

16. Garg, R.; Bahl, I.; Bozzi, M. *Microstrip Lines and Slotlines*, 3rd ed.; Artech House: Norwood, MA, USA. Available online: http://us.artechhouse.com/Microstrip-Lines-and-Slotlines-3rd-Edition-P1579.aspx (accessed on 23 April 2018).

17. Rance, O.; Siragusa, R.; Lemaître-Auger, P.; Perret, E. Contactless characterization of coplanar stripline discontinuities by RCS measurement. *IEEE Trans. Antennas Propag.* **2017**, *65*, 251–257. [CrossRef]